Journal of
NANOSTRUCTURES
JNS
NANOSTRUCTURES
JNS.kashanu.ac.ir

# Investigation of Laminar Pulsating Nanofluid Flow and Heat Transfer in a Rectangular Channel

**M. Ziaei-Rad, P. Elyasi***

*Mechanical Engineering Department, Faculty of Engineering, Shahrekord University, Shahrekord, Iran*

*Article history:*
Received 22/9/2013
Accepted 3/11/2013
Published online 1/12/2013

*Keywords:*
Pulsating flow
Nanofluid
rectangular channel
unsteady state
Numerical study

**Corresponding author:*
E-mail address:
paymanelyasi@gmail.com

**Abstract**

In this study, two-dimensional pulsating unsteady flow of nanofluid through a rectangular channel with isothermal walls is investigated numerically. The set of resultant algebraic equations is solved simultaneously using SIMPLE algorithm to obtain the velocity and pressure distribution within the channel. The effects of several parameters, such as volume fraction of different nanoparticles, Reynolds number, and the amplitude and frequency of pulsation flow, on the rate of heat transfer and pressure drop are examined. The results show that the heat transfer enhancement on the target surface obtained by the flow pulsation highly depends on pulsating velocity. It can also be seen that total Nusselt number increases significantly due to increase in amplitude of pulsation and volume fraction of nanoparticles. Analysis also reveals that pressure drop for the alumina nanoparticles is much greater than that of the base fluid.



## 1. Introduction

Pulsating flow through the different geometrical conditions is of general interest in various scientific fields [1–3]. Periodic fluctuations of fluid flow create different characteristics of flow and heat transfer. Generally, the flow fluctuations are divided into two categories: pulsating flow (or pulsatile flow) in which the periodically time-averaged velocity is non-zero and oscillating flow (or oscillatory flow) in which the periodically time-averaged velocity is zero [4]. Pulsating flows have potential for research as many aspects of such flows are still unclear and require further investigation because of many upcoming applications. Pulsating nanofluid flow and

heat transfer occur in many industrial products, such as cooling system of gas turbine engines, reciprocating engine, bio-fluid systems and thermal management of electronics etc. In addition, the flow of convective coolant in nuclear power systems in ocean environments pulsates periodically. Therefore, pulsating flow of nanofluid and its heat transfer play an important role on thermal hydraulic analysis and safety evaluation of nuclear reactors [5].

Low thermal conductivity of conventional heat transfer fluid such as water, oil and ethylene glycol mixture is a serious limitation in improving the efficiency and compactness of many engineering equipment. To overcome this disadvantage, there is a strong motivation to develop advanced heat transfer fluids with substantially higher thermal conductivity. In the past decade, nanofluids have attracted much interest because of their reported superior thermal performance and many potential applications. When nanofluid is added to this subject, it would be of great interest to researchers. Compared to micron-sized particles, nanoparticles are engineered to have larger relative surface area, less particle momentum, high mobility and better suspension stability and importantly increase the thermal conductivity of the mixture. This makes the nanofluids a promising working mediums coolants, lubricants, hydraulic fluids and metal cutting fluids. Further, a negligible pressure drop and mechanical abrasion makes researchers subscribe to nanofluids for the development of the next generation miniaturized heat exchangers. Although flow development and heat transfer in pipes and ducts is quite well studied, transport phenomena in ducts with pulsating flow condition are yet to be fully understood. A review of literature revealed some controversies about the impact of flow pulsation on the heat transfer in channels. Heat transfer in pulsating laminar flow has been studied by many investigators. However, heat transfer in pulsating flow of nanofluids is more interesting and important in practical applications. Unfortunately, it is still lacking in study.

Nield et al. [6] investigated laminar forced convection in a channel under pulsating flow using perturbation method. They presented that, although the fluctuating part of the local Nusselt number changes in magnitude and phase aspect to frequency, pulsating flow leads to no enhancement in convection rate. At an experimental and theoretical work, Shahin [7] investigated the heat transfer in a tube and also in a concentric annulus tube. His presented results showed that pulsation of flow has about 25% enhancement in heat transfer for certain frequencies of the pulsate inlet. Besides, it was demonstrated that at higher frequencies the heat transfer starts to reduce. Conversely, Chattopadhyay et al. [8] did a numerical analysis on laminar pulsating flow in a tube with constant temperature. They illustrated that pulsating flow profile has no positive outcome in heat transfer for a considered rang of frequency and pulsate amplitude. Wen and Ding [9] assessed the convective heat transfer of nanofluids in the entrance region under laminar flow conditions. Aqueous based nanofluids containing $Al_2O_3$ nanoparticles size 27–56 nm; $\phi = 0.6 - 1.6\%$ with sodium dodecyl benzene sulfonate (SDBS) as the dispersant, were tested under a constant heat flux boundary condition. For nanofluids containing $\phi = 1.6\%$, the local heat transfer coefficient in the entrance region was found to be 41% higher than that of the base fluid at the same flow rate. It was observed that the enhancement is particularly significant in the entrance region, and decreases with axial distance. Particle migration was reasoned for the enhancement. Also forced convective of a nanofluid that consists of water and $Al_2O_3$ in horizontal tubes has been studied numerically by Lotfi et al. [10]. Two-phase Eulerian, single-phase,

two-phase mixture model formulations were also used for comparison. They were illustrated that the mixture model is more precise and the single-phase model and the two-phase Eulerian model underestimates the Nusselt number. Heris et al. [11] presented an investigation of the laminar flow convective heat transfer of $Al_2O_3$–water under constant wall temperature with $\phi = 0.2 - 2.5\%$ for Reynolds number, varying between 700 and 2050. Yan et al. [12], experimentally and theoretically studied the pulsating flows in nuclear reactor which are aroused by the ship motion. The research results showed that pulsation enhanced the heat transfer and led the friction factor increases with the increase of acceleration. Jafari et al. [13] investigated the effects of the pulsating flow on forced convection in a corrugated channel; they observed that amplitude of oscillating velocity had a linear increase on heat transfer rate and the role of oscillating amplitude become more important in the extremum value of frequency. Rahgoshay et al. [14] did a numerical effort on pulsating flow of nanofluid through an isotherm pipe. They revealed that the rate of heat transfer increased slightly due to increase in the frequency and amplitude of pulsating flow. Yang and Lia [15] simulated forced convection flow of $Al_2O_3$–water nanofluid in a microchannel without any pulsation. They showed that nuselt number increased by increasing Reynolds number and volume fraction. Ghasemi and Aminossadati [16] studied numerically the problem of natural convection heat transfer in an inclined enclosure filled with a CuO-water nanofluid. The results showed that for high Rayleigh numbers, there is an optimum value for the solid volume fraction which maximized the heat transfer enhancement. Turbulent convective heat transfer performance and pressure drop of very dilute (less than 0.24% volume) CuO–water nanofluid flowing through a circular tube were investigated experimentally [17]; Measurements showed that the addition of small amounts of CuO particles to the base fluid increased heat transfer coefficients considerably. Hemida et al. [18] observed that pulsation produces little changes which is always negative in Nusselt number, i.e. heat transfer decreases for the pulsating systems. The effect of pulsation was more visible in thermally developing region as compared to the fully developed region. Guo and Sung [19] investigated the effects of pulsating flow on heat transfer in a pipe. They observed that for small amplitudes, heat transfer increased gradually due to increase in a band of operating frequency.

The above literature review does not converge to coherent conclusions. The results aren't only sparse but inconsistent and sometimes contradictory. The conclusions to this problem in this study could be classified into four different opinions: (a) flow pulsation enhances heat transfer poorly [7, 13 and 14]; it deteriorates flow and its heat transfer [18]; (c) it has no clear effect on flow and heat transfer [6 and 8]; (d) finally it either can enhance or deteriorate flow and heat transfer, depending on flow parameters [19].

Processes of heat transfer Enhancement by affecting the flow characteristics have been treated in many studies as an important goal [20–23].

Although some papers [14, 24 and 25] have investigated pulsating flow of nanofluid in a heat pipe or tube, at the knowledge of the authors this paper is the first to consider the simultaneous effect of pulsating and nanofluid in single phase forced convection in a channel.

The aim of the present paper is to demonstrate the mechanism of heat transfer in pulsating flow of nanofluids in a rectangular channel by means of a numerical solution in order to show clearly how pulsation affects the rate of heat transfer.

In this paper, the target problem is studied for different Reynolds number (Re), Strouhal number (St), volume fraction of different nanoparticles and amplitude of pulsating velocity ($A_0$) as more important parameters in the convection problem of the pulsating flow. The simulations are focused on the behavior of the unsteadiness affecting the heat transfer, velocity profile and pressure drop mechanism. At this way, the temporal and time-averaged values of cycle and space -averaged Nusselt numbers and pressure drop are presented for different case studies.

## 2. Physical and Mathematical Modeling

A rectangular channel with a pulsating source of flow placed at the inlet of the channel is considered (Fig. 1).

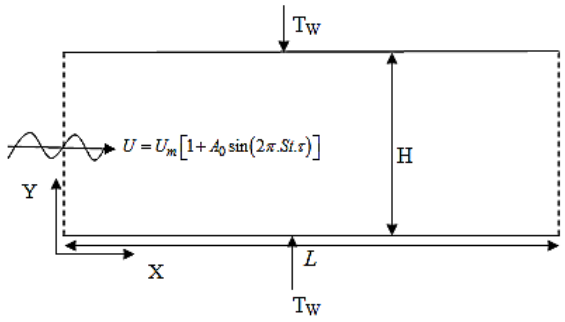


**Fig.1.** Schematic of Physical Domain

The flow enters from left-hand side with an oscillating flat velocity profile and exits from the right hand side of the physical domain. The flow is unsteady, laminar, and carries the nanoparticles. The nanoparticles and the base fluid (water) are assumed to be in a thermal equilibrium and no slip condition occurs between them. Also the body forces, radiation heat transfer and viscous dissipation are neglected in this study.

The following dimensionless variables are defined in order to represent the governing mass, momentum and energy conservation equations for laminar flow of nanofluids in non-dimensional form:

$$X = \frac{x}{H}\ , Y = \frac{y}{H}\ ,\ P = \frac{p}{\rho_f U^2_m},\ U = \frac{u}{U_m},$$

$$V = \frac{v}{U_m},\ \theta = \frac{T - T_W}{T_0 - T_W},\ \tau = \frac{tU_m}{H},\ \mathrm{Re} = \frac{U_m H}{\nu_f},$$

$$St = \frac{\vartheta H}{U_m},\ Pr = \frac{\nu_f}{\alpha_f},\ \omega = 2\pi\vartheta \qquad (1)$$

Continuity equation:

$$\frac{\partial U}{\partial X} + \frac{\partial V}{\partial Y} = 0 \qquad (2)$$

*X*-Momentum equation:

$$\frac{\partial U}{\partial \tau} + U\frac{\partial U}{\partial X} + V\frac{\partial U}{\partial Y} = -\frac{\rho_f}{\rho_{nf}}\frac{\partial P}{\partial Y} + \frac{1}{\mathrm{Re}}\frac{\rho_f}{\rho_{nf}}\frac{\mu_{nf}}{\mu_f}\left(\frac{\partial^2 U}{\partial X^2} + \frac{\partial^2 U}{\partial Y^2}\right) \qquad (3)$$

*Y*-Momentum equation:

$$\frac{\partial V}{\partial \tau} + U\frac{\partial V}{\partial X} + V\frac{\partial V}{\partial Y} = -\frac{\rho_f}{\rho_{nf}}\frac{\partial P}{\partial Y} + \frac{1}{\mathrm{Re}}\frac{\rho_f}{\rho_{nf}}\frac{\mu_{nf}}{\mu_f}\left(\frac{\partial^2 V}{\partial X^2} + \frac{\partial^2 V}{\partial Y^2}\right) \qquad (4)$$

Energy equation:

$$\frac{\partial \theta}{\partial \tau} + U\frac{\partial \theta}{\partial X} + V\frac{\partial \theta}{\partial Y} = \frac{\alpha_{nf}}{\alpha_f}\frac{1}{\mathrm{Re}.Pr}\left(\frac{\partial^2 \theta}{\partial X^2} + \frac{\partial^2 \theta}{\partial Y^2}\right) \qquad (5)$$

Where, U and V are the velocity components along the axes X and Y, respectively, P is dimensionless pressure, $\rho_{nf}$ is the effective nanofluid density, Re and Pr are Reynolds and Prandtl numbers, $\mu_{nf}$ is nanofluid effective dynamic viscosity, $\tau$ is dimensionless time, $\alpha_{nf}$ is nanofluid thermal diffusivity, $\nu_f$ is kinematic viscosity of fluid, $\omega$ is angular frequency of the motion, $\vartheta$ is dimensional frequency and $\theta$ is dimensionless temperature.

The walls have constant temperature ($T_W$) differentially lower than hot inflow temperature ($T_{in}$). The fluid enters with uniform temperature $T_{in}$. The velocity profile is obtained by adding the uniform velocity profile with a sinusoidal pulsation. So the inflow velocity profile is given by:

$$u = U_m \left[1 + A_0 \sin\left(2\pi\, St\, \tau\right)\right] \quad (6)$$

Where, $A_0$ is the amplitude of pulsating velocity and St is Strouhal number which represents the dimensionless frequency of pulsating flow. $U_m$ denotes the mean velocity of inflow.

The wall temperature is assumed to be uniform. No slip condition is also used for velocity boundary condition on the walls. The inlet velocity profile oscillates with a sinusoidal pulsation as shown in Fig. 1. Dimensionless boundary conditions can be summarized as follow:

Inlet:

$$X = 0 : U = \left[1 + A_0 \sin\left(2\pi\, St\, \tau\right)\right], V = 0,\ \theta = 1 \quad (7)$$

Top and bottom walls:

$$Y = 0,\ H \Rightarrow U = 0,\ V = 0,\ \theta = 0 \quad (8)$$

Outlet:

$$X = L :\ \partial\theta / \partial X = 0,\ \partial U / \partial X = 0,\ V = 0 \quad (9)$$

The non-dimensional flow and heat transfer parameters are defined by $\mathrm{Re} = U_m H / \nu_f$ as Reynolds number and $Nu = -\dfrac{k_{nf}.H}{\left(T_W - T_{in}\right)k_f}\left(\dfrac{\partial\theta}{\partial Y}\right)_W$ as Nusselt number.

Also cycle-averaged Nusselt and space-averaged Nusselt numbers are defined as:

$$Nu_{ca} = \frac{1}{\tau_p}\int_0^{\tau_p} Nu\, d\tau \quad (10)$$

$$Nu_{sa} = \frac{1}{L}\int_0^{L} Nu\, dX \quad (11)$$

Where, $\tau_p$ is dimensionless time period of the cycle and L is the length of the channel. The total Nusselt number and relative total Nusselt number are defined as:

$$Nu_{total} = \frac{1}{\tau_p L}\int_0^{\tau_p}\int_0^{L} Nu\, dX\, d\tau \quad (12)$$

$$Nu_{total,relative} = \frac{1}{\tau_p L}\int_0^{\tau_p}\int_0^{L} Nu.dX\, d\tau \Big/ \frac{1}{L}\int_0^{L} Nu_S\, dX \quad (13)$$

## 3. Thermophysical properties of nanofluid

### 3.1. Thermal conductivity

The thermal conductivity of nanofluid can be calculated from the following equation [26]:

$$\frac{k_{nf}}{k_f} = 1 + 64.7\phi^{0.746}\left(d_f / d_p\right)^{0.369} \times \left(k_p / k_f\right)^{0.747} \mathrm{Pr}_f^{0.9955}\, \mathrm{Re}_p^{1.23221} \quad (14)$$

Where, $\mathrm{Pr}_f = \mu_f / \rho_f \alpha_f$ is the Prandtl number of fluid, $\mathrm{Re}_p = \rho_f k_b T / 3\pi\mu^2 l_f$ is the Reynolds number of nanoparticles, $k_b$ is the Boltzmann constant, $\left(=1.3807\times10^{-23}\right)$ and $l_f$ is the free average distance of water molecules that according to Chon and et al.'s suggestion is taken as 17 nm. Some research also approved the accuracy of this model [27].

### 3.2. Density and specific heat

The density and specific heat capacity of nanofluid are defined as [28]:

$$\rho_{nf} = (1-\varphi)\rho_f + \varphi\rho_p \quad (15)$$

$$\left(\rho c_p\right)_{nf} = (1-\varphi)\left(\rho c_p\right)_f + \varphi\left(\rho c_p\right)_p \quad (16)$$

### 3.3. Viscosity

The viscosity of the nanofluid is approximated by the following correlation [29]:

$$\frac{\mu_{nf}}{\mu_f} = 1 + \rho_p V_b d_p^2 / 72 N \delta \quad (17)$$

Where, $\delta = (\pi / 6\phi)^{1/3} \times d_p$ is center to center distance of nanoparticles, $V_b = (1/d_p)\sqrt{18 k_b T / \pi \rho_p d_p}$ is Brownian velocity of nanoparticles and $N = (c_1\phi + c_2) d_p + (c_3\phi + c_4)$ is a parameter for adapting the results with experimental data when in $c_1 = -1.133 \times 10^{-6}$, $c_2 = -2.771 \times 10^{-6}$, $c_3 = 9.0 \times 10^{-8}$ and $c_4 = -3.93 \times 10^{-7}$.

The base fluid is water, which is accompanied with different types of nanoparticles such as Copper (Cu), Silver (Ag), Alumina ($Al_2O_3$), Copper oxide (CuO) and Titanate ($TiO_2$). It is assumed that the base fluid and the nanoparticles are in thermal equilibrium and no slip occurs between them. The thermo physical properties of the base fluid and nanoparticles are summarized in Table 1 [28, 30].

**Table 1.** Thermo-physical properties of water and nanoparticles.

| Base fluid and nanoparticles | ρ ($Kgm^{-3}$) | $C_p$ ($Jkg^{-1}K^{-1}$) | K ($Wm^{-1}K^{-1}$) |
|---|---|---|---|
| Pure Water($H_2O$) | 997.1 | 4179 | 0.6130 |
| Copper(Cu) | 8933 | 385.0 | 401.00 |
| CopperOxide(Cuo) | 3620 | 531.8 | 76.500 |
| Silver(Ag) | 10500 | 235.0 | 429.00 |
| alumina($Al_2O_3$) | 3970 | 765.0 | 40.000 |
| TitaniumOxide ($TiO_2$) | 4250 | 686.2 | 8.9538 |

## 4. Numerical procedure

The discretization of the governing differential equations is performed using the finite volume method [31] applied on a staggered orthogonal grid configuration. A power-law scheme is used to calculate the convective fluxes. The well-known SIMPLE algorithm [31, 32] is employed and the discretized governing equations are solved using line-by-line ADI (Alternating-Direction Implicit) iterative method. The solution of each point at each grid line is directly obtained by TDMA (TriDiagonal Matrix Algorithm). To accelerate the convergence rate, a value of 0.5 for the relaxation parameters is introduced in TDMA solver [31]. Convergence at any time-step is declared when the following criterion is met:

$$\text{for all variables:} \left|\psi^n - \psi^{n-1}\right| / \left|\psi^n\right|_{\max} \le 10^{-5} \quad (18)$$

Where, $\psi$ denotes dependent variables (u, v, p and $\theta$). The superscripts *n* and *n-1*, respectively, refer to current and previous iteration levels.

The height and length of the channel are respectively H=1 and L=10 (fig. 2) and the grid is stretched close to the channel wall to achieve to a better accuracy in numerical computations.

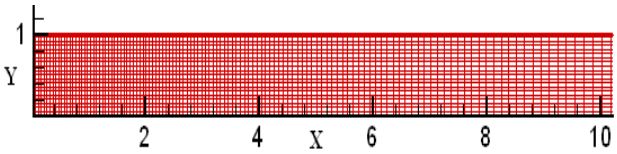


**Fig. 2.** Employed mesh geometry in the modeling.

Several grid densities (200×20, 300×20, 400×30, 400×40 and 800×40) were examined to perform a grid independency test. Figure 3 shows the velocity profile computed by different grid sizes, which leads to choose the optimum and accurate grid size of 400×40 for other numerical computations performed in this study.

In order to validate the employed computer program, a comparison between the present numerical results and available numerical results is presented in figure 4.

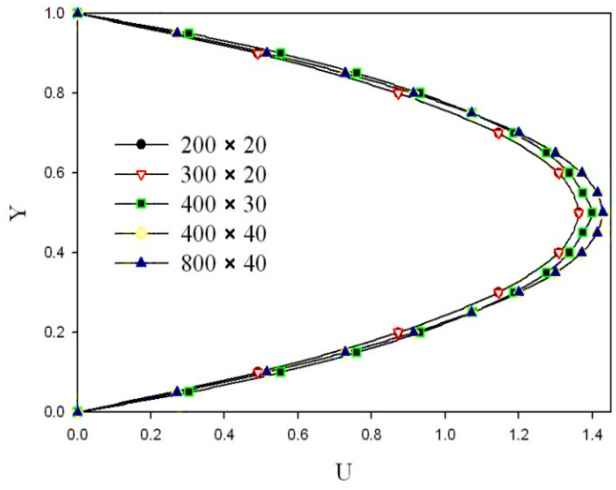


**Fig. 3.** horizontal velocity for mesh indepency investigation at Re=100 and $\phi = 0.02$ in steady State.

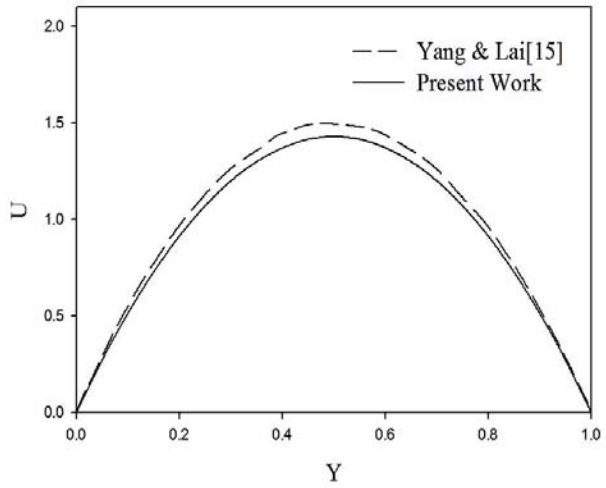


**Fig. 4.** Comparison of velocity profile in fully-developed laminar nanofluid flow in a channel with Re=16 and $\phi = 0.04$ .

The numerical result of Yang and Lia [15] for a nanofluid flow without pulsation is used as the comparison data. They computed the velocity distribution in the fully-developed laminar flow of Alumina-water nanofluid, with a Reynolds number of 16 and the volume fraction of alumina nanoparticles of $\phi = 0.04$ . The result for velocity in fully-developed channel flow is shown in fig. 4. As can be seen from the figure, the results are in good agreement indicating the accuracy of present numerical procedure.

The total Nusselt number is compared with the result of Jafari et al. [13] (table 2). It is observed from Table 2, that the present results are in good agreement with the earlier published results. This agreement confirms the accuracy of current numerical model used in simulation of velocity and temperature fields.

**Table 2.** Comparison of total Nusselt number for a pulsating flow with $\phi = 0.0$ and St= 0.1 at different amplitude of pulsation, Re = 100.

| | Total Nusselt number | |
|---|---|---|
| $A_0$ | **Present Work** | **Jafari et al.[13]** |
| 0.05 | 7.9507 | 7.8710 |
| 0.15 | 8.1562 | 8.0891 |
| 0.25 | 8.3637 | 8.3786 |

## 5. Results and discussion

The effects of the amplitude of pulsation flow (as an important parameter of pulsating flow) is investigated in Fig.5 for a pulsating flow at Re=100, St=0.1 and $\phi = 0.0$ . It can be seen that the space-averaged Nusselt number always pulsates sinusoidally, corresponding to the pulsating form of the inlet velocity. As it is expected, enhancing the amplitude of inlet velocity results in accession to the amplitude of Nusselt number diagram. It is also found that the role of pulse amplitude on heat transfer rate becomes more significant in that extremum value (see Fig. 5). When, amplitude of the velocity is 0.05, 0.15, 0.2 and 0.25, the relative total Nusselt number will gain the value of 1.0624, 1.1872, 1.2496 and 1.3123, respectively. Furthermore, the results show that increasing the amplitude of pulsation has no effect on cycle period of pulsation, while it can raise the total Nusselt

number.

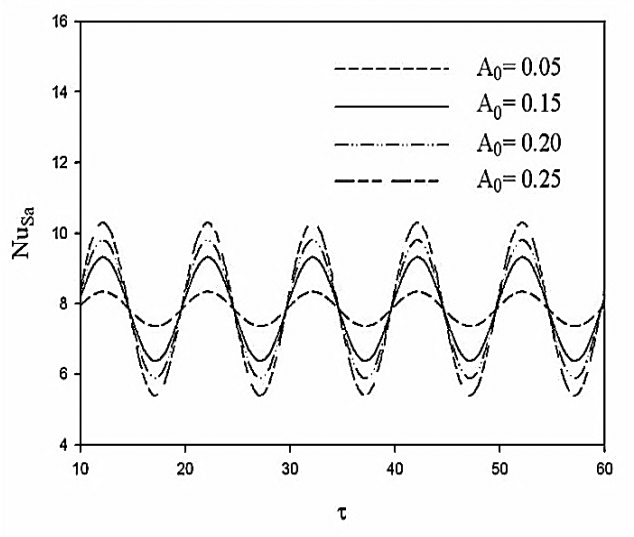


**Fig. 5.** Space-averaged Nusselt number for different amplitudes, $A_0$=0.05, 0.15, 0.20 and 0.25 at Re=100, $\phi = 0.0$ and St=0.10.

Fig. 6 shows the distribution of the cycle-averaged Nusselt number at the wall for Re=100, $A_0$=0.1, St=0.1 using four amount of nanoparticles volume fractions compared to base fluid. The figure reveals an enhancement in Nusselt number by increasing the volume fraction of nanoparticles. This behavior is explained by looking at Nusselt number definition. The effect of volume fraction of nanoparticles on the temperature gradient term and on the thermal conductivity ratio term is more pronounced than temperature difference term. Eqs. (3) to (5) show that any increase in volume fraction increases the inertia forces because the effective density of the nanofluid will be increased and accordingly increases the temperature gradient. Besides, the nanoparticles increase the thermal conductivity ratio term as it can be seen from Eq. (12). Therefore, both the temperature gradient term and thermal conductivity ratio term increase by increasing the volume fraction of nanoparticles. Accordingly, it can be seen that with increasing volume fraction the Nusselt number will be increased, because the heat transfer properties are improved. The present computations reveal that when the volume fraction increases gradually from 0.0 to 0.04, 0.06, 0.1 and 0.15 the corresponding relative total Nusselt numbers will be 1.0258, 1.1509, 1.2174, 1.3579 and 1.5503, respectively.

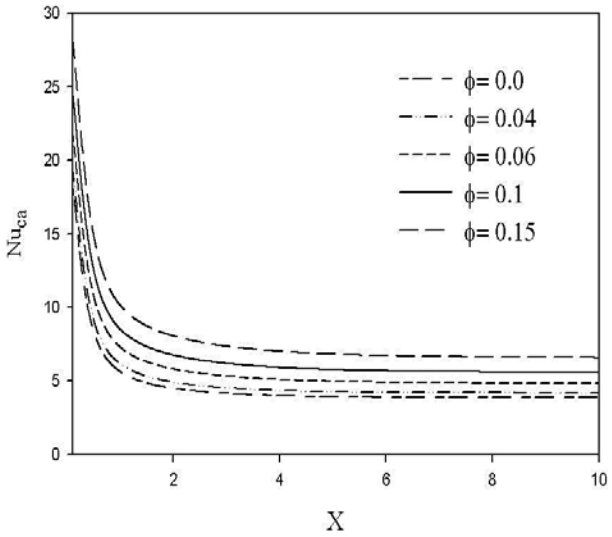


**Fig. 6.** Effect of volume fraction of nanoparticles ( $\phi$ ) on cycle-averaged Nusselt number at Re=100, $A_0$=0.1 and St=0.1.

In Fig. 7, the effect of frequency of pulsation (St) on space-averaged Nusselt number is investigated for Re=100, $A_0$=0.15 and $\phi = 0.0$. The fluid is in contact with the wall for longer time, so increasing the frequency of inlet velocity from St=0.05 to St=0.25, leads to an increase in amplitude of the space-averaged Nusselt number and its total value. When Strouhal numbers are 0.05, 0.1, 0.15 and 0.25, the relative total Nusselt numbers will be 1.1646, 1.1872, 1.2042 and 1.2241, respectively. As can be seen in this figure, the effect of Strouhal number (frequency) is not more appreciable for the heat transfer enhancement, however a slight improvement of total Nusselt number was observed. The analysis also reveals that increasing the Strouhal number reduces the cycle period of pulsation.

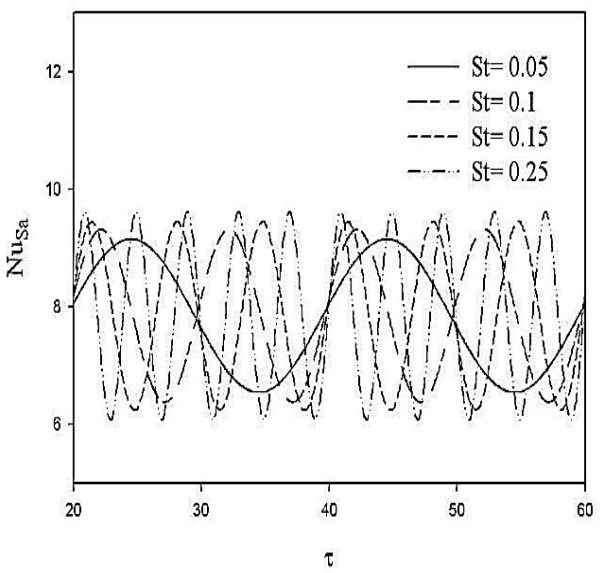


**Fig. 7.** Space averaged Nusselt number for different Strouhal Number and constant conditions Re=100, $\phi = 0.0$ and $A_0$=0.15.

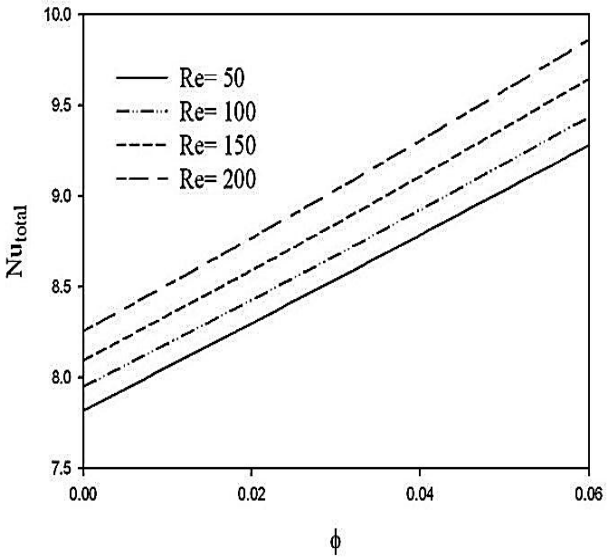


**Fig. 8.** Effect of volume fraction of nanoparticles ( $\phi$ ) and Reynolds number on total Nusselt number at A=0.05 and St=0.1.

Fig.8 demonstrates the total Nusselt number for Reynolds number of 50, 100, 150 and 200 compared to changes of volume fraction of alumina-water nanofluid. It is observed that Reynolds number strongly affects the heat transfer enhancement. Furthermore, the analysis reveals that the total Nusselt number increases significantly due to increase in volume fraction of $Al_2O_3$–water nanofluid. It can also be seen that the pulsation flow has better performance on heat transfer rate at higher Reynolds numbers.

Fig. 9 shows distribution of the horizontal velocity in the fully developed region at Re=100, $A_0$=0.2 and St=0.1 for different volume fraction of nanoparticles. It can be seen that, change in the volume fraction of alumina nanoparticle has no effect on the horizontal velocity in the fully developed region.

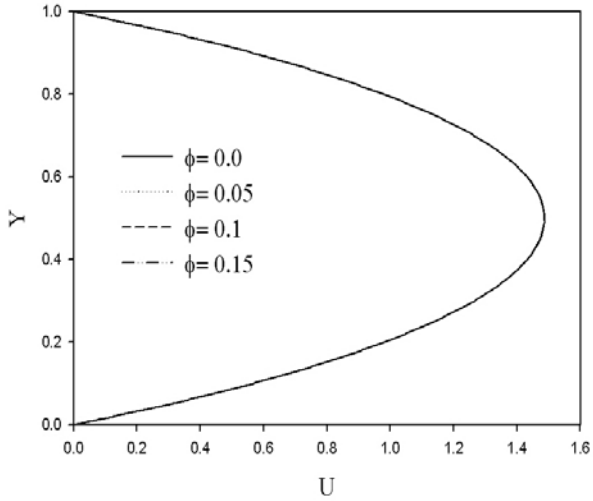


**Fig. 9.** Effect of volume fraction of nanoparticles ( $\phi$ ) on horizontal velocity in the fully developed region at Re=100, $A_0 = 0.2$ and St=0.1.

Distribution of the total Nusselt number with amplitude of 0.15 for different frequencies and volume fraction is plotted in Fig. 10. It can be readily observed that the effect of Strouhal number (frequency) is not more appreciable for the heat transfer enhancement, however a slight improvement of total Nusselt number is observed. Furthermore it

is found that by increasing volume fraction of nanofluid, the total Nusselt number raise which consequently increases the total Nusselt number.

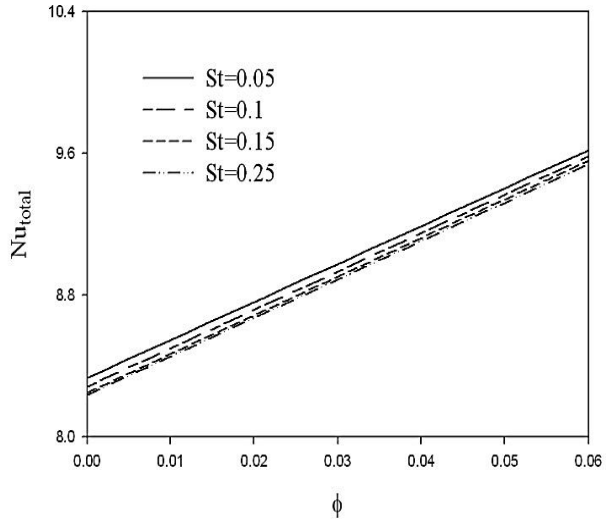


**Fig. 10.** Distribution of the total Nusselt number at $A_0$=0.15 for different St and $\phi$ .

Variations of space averaged Nusselt number against dimensionless time at $A_0$=0.1, St=0.1, Re=100 and $\phi = 0.02$ is plotted for different thermo-physical properties of water and nanoparticles (Ag, Cu, CuO, $Al_2O_3$, and $TiO_2$) in Fig. 11.

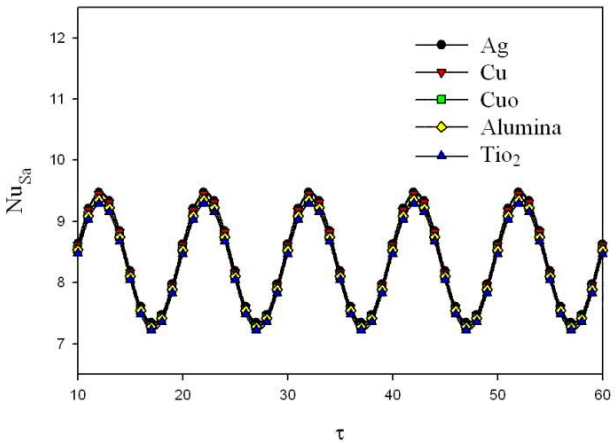


**Fig. 11.** Temporal Variation of space averaged Nusselt number for different thermo-physical properties of water and nanoparticles at $A_0$=0.1, St=0.1, Re=100 and $\phi = 0.02$ .

It can be seen that the maximum value of relative total Nusselt number for silver nanoparticles is more and titanium oxide is less than other studied nanoparticles.

Fig. 12 shows variations of pressure drop against dimensionless time at Re =100, $\phi = 0.02$ and St=0.1 for different amplitude of pulsation. It can be seen that the pressure drop always pulsates sinusoidally, corresponding to the pulsating form of the inlet velocity. It can also be seen that pressure drop varies from positive to negative and vice versa during a period due to variations of amplitude and the change of the dimensionless pressure. The analysis also reveals that the pressure drop increases significantly due to increase in amplitude of pulsation.

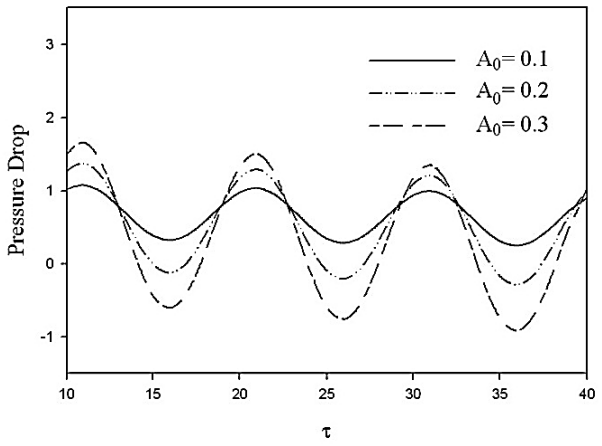


**Fig. 12.** Temporal variation of pressure drop for different amplitude of pulsation at Re=100, $\phi = 0.02$ and St=0.1.

Distribution of pressure drop with amplitude of 0.2 and frequency of pulsation 0.1 for different volume fraction of alumina nanoparticles is plotted in Fig. 13. As it can be seen in fig. 13, pressure drop is sinusoidal, which is in accord with the pulsation pattern of velocity without a phase lag. Furthermore, the result shows that the pressure drop along the horizontal walls of rectangular channel increases gradually due to increase in volume fraction of alumina nanoparticles.

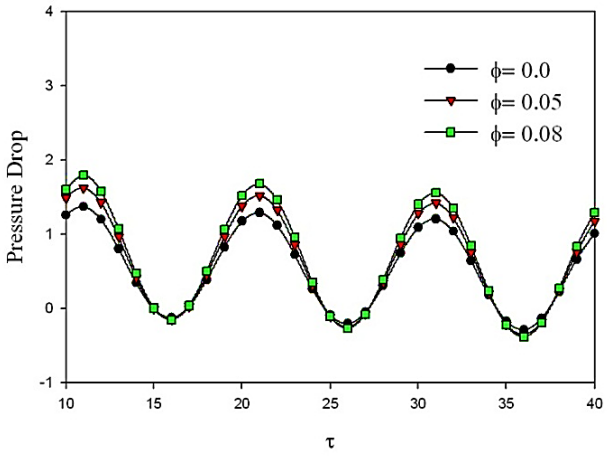


**Fig. 13.** Temporal variation of pressure for different volume fraction at Re = 100, St=0.1 and $A_0 = 0.1$.

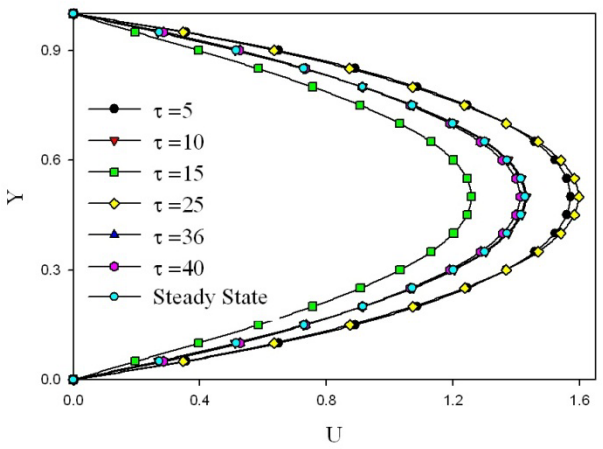


**Fig. 14.** Distribution of the horizontal velocity for different dimensionless time at X= 8.5, Y=0.45, Re=100, $A_0$=0.05, $\phi = 0.01$ and St=0.25.

Fig. 14 shows distribution of the horizontal velocity in the fully developed region at X= 8.5, Y=0.45, Re=100, $A_0$=0.05, $\phi = 0.01$ and St=0.25 for different dimensionless time. As it can be seen, the velocity at different dimensionless time varies vice versa during a period due to the change of the pressure gradient. The nanofluid velocity in a channel changes from zero at the surface because of the no-slip condition to a maximum at the channel center. The thickness of this boundary layer increases in the flow direction until the boundary layer reaches the channel center and thus fills the entire channel, as shown in Fig. 14. Near the wall, the velocity gradient becomes very large, corresponding to the boundary layer and is called the boundary region. In the buffer region between the channel center and the boundary regions, a velocity ‘‘overshoot’’ occurs at a few moments, for example, at $\tau = 5$ and 25, shown in Fig. 14. That means the flow velocity at these moments exceeds the velocity at channel center and, hence, causes larger velocity gradient at the wall than that in steady-state flow. Consequently, more heat is transported at these moments. This phenomenon is also called Richardson effect [33].

The heat transfer enhancement in the form of Nusselt number difference between pulsating flow and constant flow is tabulated in Table 3.The values of heat transfer enhancement in Table 3 clear the considerable role of extremum value of non-dimensional amplitude and volume fraction of nanofluid. It is shown that at Re=300 a pulsating flow of alumina-water nanofluid with $A_0$= 2.0 and $\phi = 0.1$ can provide a heat transfer enhancement about 60% for St= 0.1 (the extremum of $A_0$ value at Re=300) while the value of heat transfer enhancement is about 46% for $A_0$= 2.0 and $\phi = 0.0$ at same Re and St. Also, pay attention to the existing results (Table 3) which show that the performance of pulsating flow as an active technique to enhance heat transfer is entirely depending on Reynolds numbers. As an example, applying a pulsating velocity with St=0.1, $\phi = 0.0$ and $A_0$=0.5 in the rectangular channel at Re=100 makes a heat transfer enhancement about 12% while at same condition this value is about 17% and 21% respectively for Re= 200 and Re= 300. This example and other presented data in Fig. 5 and Fig. 7, clearly present that the pulsating flow becomes more effective in higher

Reynolds numbers and volume fraction of nanoparticles.

**Table 3.** Values of heat transfer enhancement at the rectangular channel using pulsating flow of alumina-water nanofluid at different conditions.

| Re | $A_0$ | $(Nu_{total}-Nu_S)/Nu_{total}\times100$ | |
|---|---|---|---|
| | | $\phi=0.0$ | $\phi=0.1$ |
| 100 | 0.5 | 11.81 | 33.16 |
| | 1.0 | 21.36 | 40.51 |
| | 1.5 | 28.98 | 46.26 |
| | 2.0 | 35.09 | 50.72 |
| 200 | 0.5 | 17.29 | 37.77 |
| | 1.0 | 28.72 | 46.59 |
| | 1.5 | 36.87 | 52.39 |
| | 2.0 | 42.85 | 56.70 |
| 300 | 0.5 | 20.88 | 40.69 |
| | 1.0 | 32.76 | 49.67 |
| | 1.5 | 40.56 | 55.25 |
| | 2.0 | 46.15 | 59.29 |

## 6. Conclusion

Pulsating flow and heat transfer of nanofluid in rectangular channel has been studied numerically. The effects of different parameters such as volume fraction of different nanoparticles (Cu, Ag, CuO, $Al_2O_3$, and $TiO_2$), Reynolds number, amplitude and frequency of pulsation flow on rate of heat transfer are investigated. The results show that pulsating velocity of nanofluid plays a considerable role on configuration of flow and thermal fields in the rectangular channel, which may lead to heat transfer enhancement. Using pulsating flow of nanofluids as an active way to enhance heat transfer is an important consequence of this study. This study also reveals that the effect of Strouhal number (frequency) is not more appreciable for the heat transfer enhancement, however a slight improvement in total Nusselt number was observed. Also, it is observed that amplitude of pulsating velocity linearly increases the heat transfer rate and that the role of pulsating amplitude is more important in the extremum values of heat transfer. Furthermore, the results show that the total Nusselt number increases significantly by increasing the volume fraction of $Al_2O_3$ nanoparticles. The maximum value of relative Nusselt number for silver nanoparticles is also more than other studied nanoparticles. The results also reveal that the pressure drop for the $Al_2O_3$-water nanofluid is much greater than that of the base fluid. Furthermore, the pressure drop increases significantly with the amplitude of pulsation and volume fraction of nanoparticles.

**Nomenclature**

$A_0$ : Amplitude of pulsating velocity
$St$ : Strouhal number (frequency of pulsation)
$U$ : Velocity components along the axes X
$V$ : Velocity components along the axes Y
$Nu$ : Nusselt number
$Re$ : Reynolds number ( $\mathrm{Re} = U_m H / \nu_f$ )
$Pr$ : Prandtl number ( $\mathrm{Pr}_f = \mu_f / \rho_f \alpha_f$ )
$P$ : Dimensionless pressure ( $P = p / \rho U_m^2$ )
$k$ : Thermal conductivity (W/m.K)
$H$ : Dimensionless height of the channel
$L$ : Dimensionless length of the channel

*Greek symbols*

$\alpha$ : Thermal diffusivity ($m^2/s$)
$\phi$ : Volume fraction (%)
$\mu$ : Effective dynamic viscosity (Pa. s)
$\rho$ : Density ($kg/m^3$)
$\tau$ : Dimensionless time
$\theta$ : Dimensionless temperature
$\omega$ : Dimensionless angular frequency ( $\omega = 2\pi St$ )
$\nu$ : Kinematic viscosity ($m^2\ s^{-1}$)
$\vartheta$ : Dimensional frequency $\left(Hz \approx s^{-1}\right)$

Subscripts

$Ca$ : Cycle-averaged
$f$ : Base fluid

*in* : Inlet
*W* : Wall
*p* : Particle
*nf* : Nanofluid
*S* : Steady state
*Sa* : Space-averaged
*m* : Average

## References

[1] D. Xu, T. Chen, Y. Xuan, Int. J. Heat and Mass Transfer, 39 (2012) 504–508.

[2] J. Galindo, P. Fajardo, R. Navarro, Applied Energy, 103 (2013) 116–127.

[3] B.H. Yan, Annals of Nuclear Energy, 38 (2011) 2779–2786.

[4] X.Wang, N. Zhang, Int. J. Heat and Mass Transfer, 48 (2005) 3957–3970.

[5] W. Chang, G. Pu-zhen, T. Si-chao, X. Chao, Int. J. Nuclear Energy, 58 (2012) 45–51.

[6] D.A. Nield, A.V. Kuznetsov, Int. J. Thermal Sciences, 46 (2007) 551–560.

[7] G.A. Shahin, MsC thesis University of Western Ontario, Ontario, 1998.

[8] H. Chattopadhyay, F. Durst, S. Ray, Int. J. Heat and Mass Transfer, 33 (2006) 475–481.

[9] D. Wen, Y. Ding, Int .J. Heat and Mass Transfer, 47 (2004) 5181–5188.

[10] R. Lotfi, Y. Saboohi, A.M. Rashidi, Int. J. Heat and Mass Transfer, 37 (1) (2009) 74–78.

[11] S.Z. Heris, M.N. Esfahany, S.Gh. Etemad, Int. J. Heat and Fluid Flow, 28 (2) (2007) 203–210.

[12] Yan, B.H., Yu, L., Yang, Y.H., Ann. Nucl. Energy 37, (2010) 295-301.

[13] M. Jafari, M. Farhadi, K. Sedighi, Int. J. Heat and Mass Transfer, 45 (2013) 146–154.

[14] M. Rahgoshay, A.A. Ranjbar, A. Ramiar, Int. J. Heat and Mass Transfer, 39 (2012) 463–469.

[15] Y. T., Yang, F.H, Lai, Int.J.Heat and Mass Transfer, 38 (2011) 607–614.

[16] B. Ghasemi, S.M. Aminossadati, Int. J.Heat Transfer. Part A, 55 (2009) 807–823.

[17] S.M. Fotukian, M. Nasr Esfahany, Int. J. Heat and Mass Transfer, 37 (2010) 214–219.

[18] H.N. Hemida, M.N. Sabry, A. Abbel-Rahim, H. Mansour, Int. J. Heat and Mass Transfer, 45 (2002) 1767–1780.

[19] Z. Guo, H. J. Sung, Int. J. Heat and Mass Transfer, 40 (1997) 2486-2489,

[20] A. Kumar, A.K. Dhiman, Int. J. Thermal Sciences, 52 (2012) 176–185.

[21] P. Promvonge, S. Pethkool, M. Pimsarn, C. Thianpong, Int. J. Heat and Mass Transfer, 39 (7) (2012) 953–959.

[22] H.A. Mohammed, P. Gunnasegaran, N.H. Shuaib, Int. J. Heat and Mass Transfer, 38 (1) (2011) 63–68.

[23] H. Heidary, M.J. Kermani, Int. J. Heat and Mass Transfer, 39 (1) (2012) 112–120.

[24] Y.H. Lin, S.W. Kang, H.L. Chen, Applied Thermal Engineering, 28 (2008) 1312–1317.

[25] R.R. Riehl, N.D. Santos, Applied Thermal Engineering, (2011) 1–5.

[26] C.H. Chon, K.D. Kihm, S.P. Lee, S.U.S. Choi, Applied Physics Letters, 87 (15) (2005) 153107–153110.

[27] H.A. Mintsa, G. Roy, C.T. Nguyen, D. Doucet, Int. J. Thermal Sciences, 48 (2009) 363–371.

[28] A. Mahdy, Nuclear Engineering and Design, 249 (2012) 248-255.

[29] N. Masoumi, N. Sohrabi, A.A. Behzadmehr, J. Phys, D: Applied Physics 42, (2009) 055501–055506.

[30] Oztop, H.F., Abu-Nada, E., Int. J. Heat Fluid Flow, 29 (2008) 1326–1336.

[31] S.V. Patankar, Hemisphere Publishing Corporation, New York, (1980).

[32] J.P. Van Doormaal, G.D. Raithby Int. J. Heat Transfer, 7 (1984) 147–163.

[33] S. Uchida, ZAMP, 7 (1956) 403–422.